

# Steam Reforming of Dimethoxymethane, Methanol and Dimethyl Ether on CuO–ZnO/ $\gamma$ -Al<sub>2</sub>O<sub>3</sub> Catalyst<sup>1</sup>

A. A. Pechenkin<sup>a, b, \*</sup>, S. D. Badmaev<sup>a, b</sup>, V. D. Belyaev<sup>a</sup>, E. A. Paukshtis<sup>a</sup>,  
O. A. Stonkus<sup>a, b</sup>, and V. A. Sobyenin<sup>a</sup>

<sup>a</sup>Boriskov Institute of Catalysis, Siberian Branch, Russian Academy of Sciences,  
pr. Acad. Lavrentieva 5, Novosibirsk, 630090 Russia

<sup>b</sup>Novosibirsk State University, Pirogova st. 2, Novosibirsk, 630090 Russia

\*e-mail: pechenkin@catalysis.ru

Received December 12, 2016

**Abstract**—The performance of a CuO–ZnO/ $\gamma$ -Al<sub>2</sub>O<sub>3</sub> catalyst for the reactions of methanol, dimethyl ether (DME) and dimethoxymethane (DMM) steam reforming (SR) to hydrogen-rich gas was studied. The catalyst was found to be active and selective for methanol and DMM SR producing hydrogen-rich gas with low content of CO (<1 vol %). It provided complete conversion of methanol and DMM at 300°C, and hydrogen productivity of, respectively, 15 and 16.5 L<sub>H<sub>2</sub></sub> g<sub>cat</sub><sup>-1</sup> h<sup>-1</sup>. With the use of physicochemical methods and catalytic experiments, it was shown that the catalyst surface contained the acid sites typical for  $\gamma$ -Al<sub>2</sub>O<sub>3</sub>, and CuO–ZnO agglomerates, responsible, respectively, for DMM hydration to methanol and formaldehyde, and SR of these compounds to hydrogen-rich gas.

**Keywords:** hydrogen, dimethoxymethane, methanol, dimethyl ether, steam reforming, copper-zinc catalysts, fuel cells

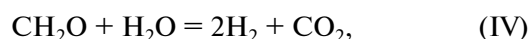
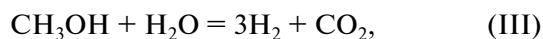
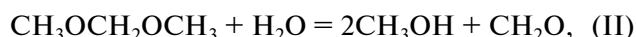
**DOI:** 10.1134/S0023158417050196

Power units based on low- and high-temperature proton-exchange membrane fuel cells (PEMFC) are considered as alternative ecologically benign sources of electric power for various applications [1–5]. PEMFCs are fuelled by hydrogen or hydrogen-rich gas which can be generated by catalytic steam reforming of oxygenated organic compounds.

In particular, scientists concentrated considerable efforts on the synthesis of hydrogen-rich gas for PEMFC feeding from methanol and DME [6–15]. It was proved that methanol and DME can be converted selectively to hydrogen-rich gas at relatively low temperature (250–350°C). Efficient methanol and DME SR catalysts were developed and used to create “fuel processors” (i.e., hydrogen-rich gas generators).

DMM, similarly to methanol and DME, is a readily synthesized oxygenated compound of C<sub>1</sub> chemistry. Since DMM is noncorrosive and nontoxic material, it is easily stored, transported, widely used [16, 17], and considered [18–23] as a promising source of hydrogen-rich gas for PEMFC feeding applications (together with methanol and DME).

According to [18–23], DMM SR (I) proceeds at 250–300°C by consecutive kinetic scheme including DMM hydration to methanol and formaldehyde (II) and SR of the formed methanol (III) and formaldehyde (IV) to hydrogen-rich gas. During DMM SR, a formation of CO by RWGS reaction (V) can occur as well.



It is generally assumed that the solid acid catalysts (acid sites) are responsible for DMM hydration, whereas the Cu-based catalysts (Cu-containing sites), for methanol/formaldehyde SR.

As reported in our recent paper [23], the CuO–ZnO/ $\gamma$ -Al<sub>2</sub>O<sub>3</sub> catalysts were active and selective for DMM SR. Comparative analysis of the catalytic performance of  $\gamma$ -Al<sub>2</sub>O<sub>3</sub>, ZnO/ $\gamma$ -Al<sub>2</sub>O<sub>3</sub>, CuO/ $\gamma$ -Al<sub>2</sub>O<sub>3</sub> and CuO–ZnO/ $\gamma$ -Al<sub>2</sub>O<sub>3</sub> under DMM SR conditions allowed suggestion that the acid sites of  $\gamma$ -Al<sub>2</sub>O<sub>3</sub> were responsible for DMM hydration to methanol and formaldehyde (II), whereas Cu–Zn oxide was respon-

<sup>1</sup> The article was translated by the authors.

sible for the formed methanol (III)/formaldehyde (IV) SR to hydrogen-rich gas.

In the present paper which is a continuation of [23], the results on the DMM SR performance of  $\gamma$ -Al<sub>2</sub>O<sub>3</sub>, 5 wt % ZnO/ $\gamma$ -Al<sub>2</sub>O<sub>3</sub> and 10 wt % CuO–5 wt % ZnO/ $\gamma$ -Al<sub>2</sub>O<sub>3</sub> are presented in more detail. Physicochemical characterization of the samples, including identification of the nature of active sites on the catalyst surface, was performed using the following techniques: BET, XRD, TPR, FTIR spectroscopy, HAADF-STEM and EDX. Besides, the data on the catalytic properties of 10 wt % CuO–5 wt % ZnO/ $\gamma$ -Al<sub>2</sub>O<sub>3</sub> in methanol SR and DME SR are given. Based on these data, the analysis is performed whether this catalyst is suitable for developing a multi-fuel processor generating hydrogen-rich gas from DMM, methanol and DME for PEMFC feeding applications.

## EXPERIMENTAL

10 wt % CuO–5 wt % ZnO/ $\gamma$ -Al<sub>2</sub>O<sub>3</sub> (denoted hereinafter as CuO–ZnO/ $\gamma$ -Al<sub>2</sub>O<sub>3</sub>) was prepared by incipient wetness co-impregnation of  $\gamma$ -Al<sub>2</sub>O<sub>3</sub> ( $S_{\text{BET}} = 200 \text{ m}^2/\text{g}$ ,  $V_{\text{pore}} = 0.7 \text{ cm}^3/\text{g}$ , granule diameter 0.25–0.5 mm) with aqueous solutions of copper(II) and zinc(II) nitrates taken at the desired ratio. Catalyst 5 wt % ZnO/ $\gamma$ -Al<sub>2</sub>O<sub>3</sub> (ZnO/ $\gamma$ -Al<sub>2</sub>O<sub>3</sub> hereinafter) was prepared by incipient wetness impregnation of  $\gamma$ -Al<sub>2</sub>O<sub>3</sub> by aqueous solution of zinc(II) nitrate. The samples were dried at 100°C for 2 h and calcined at 400°C for 3 h.  $\gamma$ -Al<sub>2</sub>O<sub>3</sub> (JSC Katalizator, Russia) was calcined at 600°C for 4 h before being used as the support.

Actual CuO and ZnO loadings in the catalysts was determined by inductively coupled plasma atomic emission spectrometry using an Optima 8X00 instrument (Perkin-Elmer, USA). The specific BET surface areas ( $S_{\text{BET}}$ ) of the catalysts were calculated from the nitrogen adsorption isotherms at –196°C using a TriStar 3000 apparatus (Micromeritics, USA).

The acidity of the catalysts was determined using the IR-spectra of adsorbed CO at –196°C [24]. The catalyst in a form of a disc was placed into the IR cell, reduced in hydrogen flow, degassed in vacuum at 300–400°C, cooled to –196°C and treated with CO doses. The IR spectra were recorded on a Shimadzu FTIR-8300 spectrometer (Shimadzu, Japan) in the range of 1000–6000 cm<sup>–1</sup> with a resolution of 4 cm<sup>–1</sup>. According to this procedure, the Brønsted acid sites (BAS) and Lewis acid sites (LAS) exhibit absorption bands at 2150–2175 cm<sup>–1</sup> and 2175–2240 cm<sup>–1</sup>, respectively. The strength of BAS is characterized by proton affinity, that of LAS, by CO adsorption heat ( $Q_{\text{CO}}$ ).

The XRD pattern of the samples were recorded on a ARL X'TRA diffractometer (Thermo Fisher Scientific, Switzerland) with CuK $\alpha$ -radiation and graphite monochromator, in the scanning range of  $2\theta = 5^\circ$ – $75^\circ$  with a step of 0.01° and sampling time of 5 s. The dif-

fraction data were processed using the PowderCell 2.4 program and JCPDS database.

Temperature-programmed reduction (TPR) of the samples was performed using an STA 409 PC Luxx (NETZSCH, Germany) derivatograph equipped with a QMS-200 mass-spectrometer. The samples (~50 mg) were heated from room temperature to 400°C at a rate of 5°C/min in a 5 vol % H<sub>2</sub> + 95 vol % Ar mixture fed at 140 cm<sup>3</sup>/min. During these experiments, variation in the hydrogen concentration was registered by the mass-spectrometer.

The analysis of the surface composition and compositional homogeneity of the supported particles was performed using a high-angle annular dark field scanning transmission electron microscopy (HAADF-STEM) images and energy-dispersive X-ray (EDX) patterns. The experiments were performed using an electron microscope JEM2200FS (“JEOL,” Japan) fitted with a HAADF detector to obtain images of high atomic contrast in scanning mode, and with EDX-analyzer for local microanalysis and EDX-local mapping.

DMM, methanol and DME steam reforming reactions were studied in a quartz U-shaped continuous-flow reactor (i.d. 4 mm, wall thickness 1 mm) at 150–370°C under atmospheric pressure. Catalyst loadings in the reactor were ~0.3–0.4 g, granule diameter – 0.25–0.50 mm. The temperature was measured with a chromel–alumel thermocouple placed in the center of the catalyst bed. The catalysts were exposed to the feed compositions (vol %): 14 DMM, 70 H<sub>2</sub>O and 16 N<sub>2</sub>; 40 CH<sub>3</sub>OH, 40 H<sub>2</sub>O and 20 N<sub>2</sub>; 20 DME, 60 H<sub>2</sub>O and 20 N<sub>2</sub> supplied at GHSV of 10000 h<sup>–1</sup> (~16 L g<sub>cat</sub><sup>–1</sup> h<sup>–1</sup>). Prior experiments, the catalysts were reduced in a flow of 5 vol % H<sub>2</sub> + 95 vol % N<sub>2</sub> mixture at 300°C for 1 h.

The inlet and outlet gas compositions were analyzed by a gas chromatograph Chromos-1000 (Russia) fitted with TCD/FID detectors and Porapack T and CaA columns. The procedure allowed detection of methanol, DMM, DME, H<sub>2</sub>, CO, CO<sub>2</sub> and methyl formate with a sensitivity of  $\leq 5 \times 10^{-3}$  vol %. Carbon imbalance was less than 3 relative percent. The data were reproducible in several cycles of rising/lowering the temperature.

The DMM conversion ( $X_{\text{DMM}}$ , %) and hydrogen productivity ( $W_{\text{H}_2}$ , L g<sub>cat</sub><sup>–1</sup> h<sup>–1</sup>) were calculated using the following equations:

$$X_{\text{DMM}} = \frac{C_{\text{DMM}}^0 - C_{\text{DMM}}}{C_{\text{DMM}}^0} \frac{C_{\text{N}_2}^0}{C_{\text{N}_2}} \times 100,$$

$$W_{\text{H}_2} = \frac{FC_{\text{H}_2} \frac{C_{\text{N}_2}^0}{C_{\text{N}_2}}}{100m},$$

**Table 1.** Physicochemical characteristics of the catalysts

Catalyst	Content, wt %				$S_{\text{BET}}$ , m <sup>2</sup> /g	$N_{\text{LAS}}$ , μmol/g	$Q_{\text{CO}}$ , kJ/mol
	calculated		experiment				
	CuO	ZnO	CuO	ZnO			
$\gamma\text{-Al}_2\text{O}_3$	–	–	–	–	200	600	30
ZnO/ $\gamma\text{-Al}_2\text{O}_3$	–	5	–	4.4	180	430	29
CuO–ZnO/ $\gamma\text{-Al}_2\text{O}_3$	10	5	9.6	4.5	160	240	28

where  $C^0$  and  $C$  are the inlet and outlet concentrations (vol %), respectively,  $F$  is the total flow rate of the inlet reaction mixture (L/h),  $m$  is the catalysts weight (g).

## RESULTS AND DISCUSSION

### Catalyst Characterization

Table 1 presents the calculated and actual CuO and ZnO loadings,  $S_{\text{BET}}$ , acidic properties (LAS concentration ( $N_{\text{LAS}}$ ) and CO adsorption heat ( $Q_{\text{CO}}$ )) for the studied catalysts. It is seen that the calculated CuO and ZnO loadings are similar to the actual values.  $S_{\text{BET}}$  decreases from 200 m<sup>2</sup>/g ( $\gamma\text{-Al}_2\text{O}_3$ ) to 180 m<sup>2</sup>/g (ZnO/ $\gamma\text{-Al}_2\text{O}_3$ ) and 160 m<sup>2</sup>/g (CuO–ZnO/ $\gamma\text{-Al}_2\text{O}_3$ ).  $\gamma\text{-Al}_2\text{O}_3$ , ZnO/ $\gamma\text{-Al}_2\text{O}_3$  and CuO–ZnO/ $\gamma\text{-Al}_2\text{O}_3$  are the solid Lewis acids. The LAS concentration is 600 μmol/g for  $\gamma\text{-Al}_2\text{O}_3$ , and 430 and 240 μmol/g for ZnO/ $\gamma\text{-Al}_2\text{O}_3$  and CuO–ZnO/ $\gamma\text{-Al}_2\text{O}_3$ , respectively. Judging by similar  $Q_{\text{CO}}$  values, the LAS strength in the studied samples is the same. Note also that some BAS (<20 μmol/g) were detected on the  $\gamma\text{-Al}_2\text{O}_3$  surface, and no BAS – on ZnO/ $\gamma\text{-Al}_2\text{O}_3$  and CuO–ZnO/ $\gamma\text{-Al}_2\text{O}_3$ .

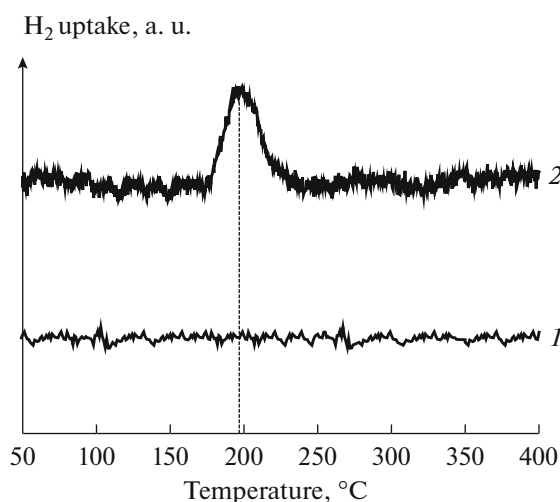
The XRD patterns of  $\gamma\text{-Al}_2\text{O}_3$ , fresh (i.e., prior reduction and DMM SR experiments) and used CuO–ZnO/ $\gamma\text{-Al}_2\text{O}_3$  (i.e., after DMM SR experiments) catalysts showed only peaks characteristic for  $\gamma\text{-Al}_2\text{O}_3$ . No diffraction peaks corresponding to Cu, Zn, CuO and ZnO were observed – most likely, these species present on  $\gamma\text{-Al}_2\text{O}_3$  surface in highly dispersed state [25]. According to calculations, the unit cell parameter of  $\gamma\text{-Al}_2\text{O}_3$  was 7.918 Å, the size of coherent-scattering region (CSR) equaled 45 Å. Compared to  $\gamma\text{-Al}_2\text{O}_3$ , CuO–ZnO/ $\gamma\text{-Al}_2\text{O}_3$  (fresh and used) demonstrated somewhat higher values of the lattice parameter and CSR size, which equaled 7.924 and 50 Å, respectively, more intensive peak at  $2\theta \approx 37^\circ$  and almost no peak at  $2\theta \approx 39^\circ$ . These facts allow suggestion that copper and zinc cations may insert into alumina lattice to form mixed spinel-type phases.

Figure 1 presents the H<sub>2</sub>-TPR profiles of fresh ZnO/ $\gamma\text{-Al}_2\text{O}_3$  and CuO–ZnO/ $\gamma\text{-Al}_2\text{O}_3$  catalysts. It is seen that ZnO/ $\gamma\text{-Al}_2\text{O}_3$  uptakes no hydrogen; CuO–ZnO/ $\gamma\text{-Al}_2\text{O}_3$  demonstrates one hydrogen uptake peak at  $\sim 190^\circ\text{C}$ . According to [26], such a low reduction temperature most likely means that CuO particles

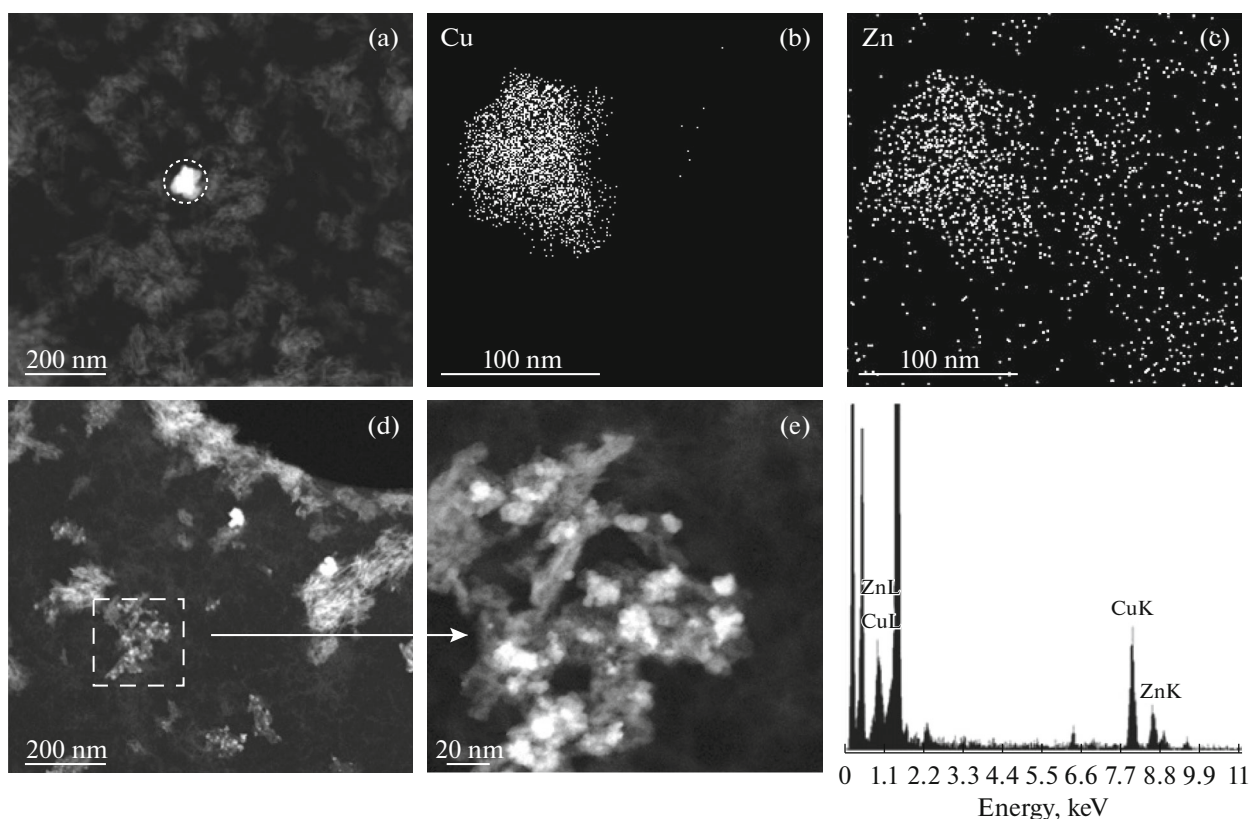
exist on the support surface in a form of well dispersed species, in good agreement with the above XRD data. Calculated hydrogen uptake at TPR of CuO–ZnO/ $\gamma\text{-Al}_2\text{O}_3$  proved complete reduction of the supported CuO to metallic copper.

Figure 2 presents the results of the HAADF-STEM and EDX studies of fresh and spent CuO–ZnO/ $\gamma\text{-Al}_2\text{O}_3$  catalysts. The HAADF-STEM image of fresh CuO–ZnO/ $\gamma\text{-Al}_2\text{O}_3$  (Fig. 2a) demonstrates only large agglomerates (white patches) of size 80–100 nm. EDX-maps (Figs. 2b, 2c) indicate simultaneous presence of copper and zinc. According to EDX microanalysis, atomic ratio Cu/Zn  $\approx 2$ , being almost equal to that value calculated from the chemical composition data (Table 1). The HAADF-STEM images of spent CuO–ZnO/ $\gamma\text{-Al}_2\text{O}_3$  (Figs. 2d, 2e) show both large ( $\sim 50\text{--}80$  nm) and small ( $\sim 20$  nm) species. Figure 2f demonstrates EDX-spectrum for the spot with small species. It is seen that atomic ratio Cu/Zn  $\approx 2$ .

The above TPR and XRD data allow suggestion that agglomerates in fresh catalyst consist of well-dispersed copper and zinc oxide species, whereas the used catalyst contains fine-dispersed particles of metallic copper and zinc oxide.



**Fig. 1.** H<sub>2</sub> uptake at TPR of fresh ZnO/ $\gamma\text{-Al}_2\text{O}_3$  (1) and CuO–ZnO/ $\gamma\text{-Al}_2\text{O}_3$  (2). Dotted line indicates the maximum of H<sub>2</sub> absorption on CuO–ZnO/ $\gamma\text{-Al}_2\text{O}_3$ .



**Fig. 2.** HAADF-STEM micro-image (a) and EDX-mapping (distribution) Cu (b) and Zn (c) of a selected patch on fresh CuO–ZnO/ $\gamma$ -Al<sub>2</sub>O<sub>3</sub>. HAADF-STEM micro-image (d, e) and EDX-spectrum (f) of the selected patch on CuO–ZnO/ $\gamma$ -Al<sub>2</sub>O<sub>3</sub> after DMM SR.

Thus, the results obtained allow conclusion that operating catalyst CuO–ZnO/ $\gamma$ -Al<sub>2</sub>O<sub>3</sub> (i.e., reduced and exposed to DMM SR conditions) possesses bifunctional activity. The catalyst surface contains active sites of two types: LAS (typical for  $\gamma$ -Al<sub>2</sub>O<sub>3</sub> and, most likely, responsible for DMM hydration to methanol and formaldehyde) and a 20–80 nm agglomerates with atomic ratio Cu/Zn  $\approx$  2 (responsible, most likely, for methanol and formaldehyde SR to hydrogen-rich gas).

*DMM SR on  $\gamma$ -Al<sub>2</sub>O<sub>3</sub>, ZnO/ $\gamma$ -Al<sub>2</sub>O<sub>3</sub>  
and CuO–ZnO/ $\gamma$ -Al<sub>2</sub>O<sub>3</sub>*

Under DMM SR conditions,  $\gamma$ -Al<sub>2</sub>O<sub>3</sub> and ZnO/ $\gamma$ -Al<sub>2</sub>O<sub>3</sub> catalyze mainly the formation of methanol and formaldehyde (i.e., DMM hydration, reaction (II)). Note that at temperatures exceeding 225–250°C, small amounts (0.5–2.0 vol %) of DME and methyl formate are formed, most likely, by the following reactions:

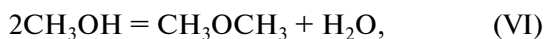


Figure 3 shows the temperature dependencies of DMM conversion and product concentrations (metha-

nol and formaldehyde) at DMM hydration on  $\gamma$ -Al<sub>2</sub>O<sub>3</sub> and ZnO/ $\gamma$ -Al<sub>2</sub>O<sub>3</sub>. Besides, it presents the equilibrium values of DMM conversion and methanol/formaldehyde concentrations calculated on the assumption that only DMM hydration (reaction (II)) proceeds in the system. Obviously, both catalysts demonstrate similar dependencies. As the temperature increases from 150 to 250–280°C, the DMM conversion and methanol concentration increase and approach equilibrium values (100% and 23.8 vol %, respectively). Note that methanol concentration slightly under-reaches the equilibrium value due to side-reaction of methanol dehydration to DME (VI). With increasing temperature, formaldehyde concentration first increases, tends to reach the equilibrium value, and then decreases. The latter observation is most likely explained by the presence of reaction (VII) which was ignored at the calculation of the equilibrium composition.

Compared to  $\gamma$ -Al<sub>2</sub>O<sub>3</sub>, the ZnO/ $\gamma$ -Al<sub>2</sub>O<sub>3</sub> curves in Fig. 3 are shifted towards higher temperatures. This fact means that  $\gamma$ -Al<sub>2</sub>O<sub>3</sub> is more active in DMM hydration than ZnO/ $\gamma$ -Al<sub>2</sub>O<sub>3</sub>. Since DMM hydration proceeds on the acid sites, this observation is quite expectable, because the acid sites concentration on  $\gamma$ -Al<sub>2</sub>O<sub>3</sub> exceeded that value for ZnO/ $\gamma$ -Al<sub>2</sub>O<sub>3</sub> (Table 1), whereas the TOF values of both catalysts at 175°C

(DMM conversion  $\leq 15\%$ ) appeared almost the same for ( $6.0 \times 10^{-3} \text{ s}^{-1}$  for  $\gamma\text{-Al}_2\text{O}_3$  and  $5.3 \times 10^{-3} \text{ s}^{-1}$  for  $\text{ZnO}/\gamma\text{-Al}_2\text{O}_3$ ).

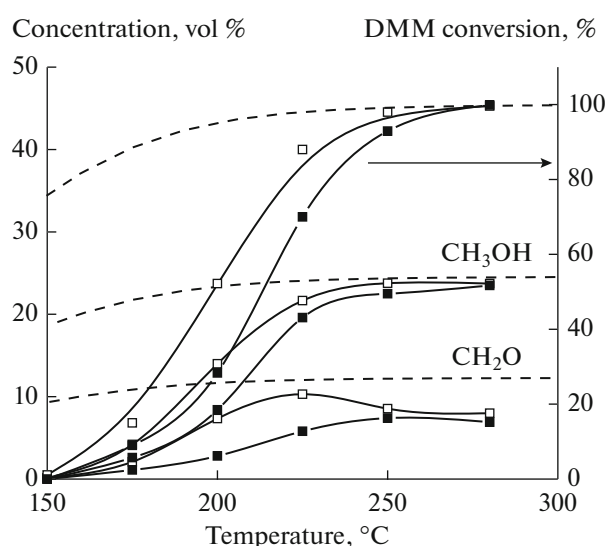
In contrast to  $\gamma\text{-Al}_2\text{O}_3$  and  $\text{ZnO}/\gamma\text{-Al}_2\text{O}_3$ ,  $\text{CuO}-\text{ZnO}/\gamma\text{-Al}_2\text{O}_3$  is active for DMM SR to hydrogen-rich gas, because this catalyst possesses bifunctional activity (see previous Section). It contains the surface acid sites typical for  $\gamma\text{-Al}_2\text{O}_3$ , which are responsible for DMM hydration to methanol and formaldehyde, and copper-containing species (agglomerates of highly-dispersed metallic copper and zinc oxide), which catalyze SR of DMM hydration products to hydrogen-rich gas.

Figure 4 shows the temperature dependencies of DMM conversion and product concentrations ( $\text{H}_2$ ,  $\text{CO}_2$ ,  $\text{CO}$  and  $\text{CH}_3\text{OH}$ ) at DMM SR on  $\text{CuO}-\text{ZnO}/\gamma\text{-Al}_2\text{O}_3$ , as well as the equilibrium values of DMM conversion and  $\text{H}_2$ ,  $\text{CO}_2$  and  $\text{CO}$  concentrations. The equilibrium concentrations of  $\text{CH}_3\text{OH}$ ,  $\text{CH}_2\text{O}$ , DME and DMM were below  $6 \times 10^{-3} \text{ vol } \%$  and are not shown in Fig. 4.

It is seen that the DMM conversion increases with increasing temperature and reaches 100% at temperatures above  $250^\circ\text{C}$ . The curve of methanol concentration passes through maximum at  $200^\circ\text{C}$  and then decreases to zero, in good agreement with the suggested kinetic scheme of DMM SR assuming methanol formation as an intermediate product (reactions (II)–(IV)). Methanol is formed by the DMM hydration reaction (II) on the acid sites of  $\gamma\text{-Al}_2\text{O}_3$  and is consumed by SR reaction (III) on the Cu-based sites. Note that formaldehyde (another intermediate formed by reaction (II)) is detected only in trace amount ( $\leq 10^{-2} \text{ vol } \%$ ). There is no contradiction with the suggested kinetic scheme, because formaldehyde is more active for SR reactions compared to methanol [27].

Concentrations of  $\text{H}_2$ ,  $\text{CO}_2$  and  $\text{CO}$  increase with increasing temperature (Fig. 4). At  $280\text{--}300^\circ\text{C}$ , the  $\text{H}_2$  and  $\text{CO}_2$  concentrations slightly exceed the equilibrium values, while the  $\text{CO}$  concentration ( $0.9 \text{ vol } \%$ ) is below the equilibrium one. This observation is most likely explained by that  $\text{H}_2$  and  $\text{CO}_2$  are the primary products of reactions (III) and (IV), whereas  $\text{CO}$  is formed by reaction (V). Obviously, if reaction (V) does not reach equilibrium during the experiment, the  $\text{H}_2$  and  $\text{CO}_2$  concentrations should exceed, and the  $\text{CO}$  concentration should be below the corresponding equilibrium values.

The results presented in Fig. 4 prove that complete DMM conversion is reached in the temperature range of  $280\text{--}300^\circ\text{C}$ , yielding  $\text{H}_2$ ,  $\text{CO}_2$  and  $\text{CO}$  as the main reaction products. Under these conditions, the catalyst demonstrates the maximum productivity of  $\sim 16.5 \text{ L}_{\text{H}_2} \text{ g}_{\text{cat}}^{-1} \text{ h}^{-1}$ , the  $\text{CO}$  concentration in the hydrogen-rich gas is below  $0.9 \text{ vol } \%$ .



**Fig. 3.** Temperature dependencies of methanol and formaldehyde concentrations, and DMM conversion at DMM hydration on  $\gamma\text{-Al}_2\text{O}_3$  ( $\square$ ) and  $\text{ZnO}/\gamma\text{-Al}_2\text{O}_3$  ( $\blacksquare$ ). Experimental conditions: pressure 1 atm, GHSV  $10000 \text{ h}^{-1}$ , inlet mixture composition (vol %) DMM :  $\text{H}_2\text{O}$  :  $\text{N}_2$  (14 : 70 : 16). Points stand for experiment, dotted lines stand for equilibrium values.

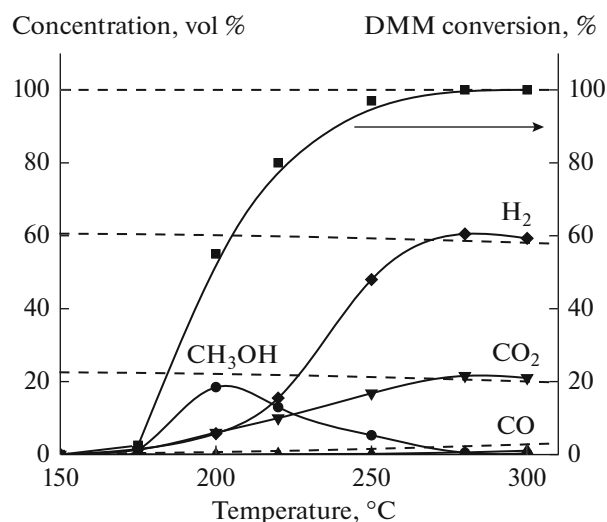


**Fig. 4.** Temperature dependencies of  $\text{H}_2$ ,  $\text{CO}_2$  and  $\text{CO}$  concentrations and DMM conversion at DMM SR on  $\text{CuO}-\text{ZnO}/\gamma\text{-Al}_2\text{O}_3$ . Experimental conditions: pressure 1 atm, GHSV  $10000 \text{ h}^{-1}$ , inlet mixture composition (vol %) DMM :  $\text{H}_2\text{O}$  :  $\text{N}_2$  (14 : 70 : 16). Points stand for experiment, dotted lines stand for equilibrium values.

#### DME SR and Methanol SR on $\text{CuO}-\text{ZnO}/\gamma\text{-Al}_2\text{O}_3$

$\text{H}_2$ ,  $\text{CO}_2$  and  $\text{CO}$  were the main products at DME and methanol SR. Figures 5 and 6 present the temperature dependencies of DME and methanol conver-

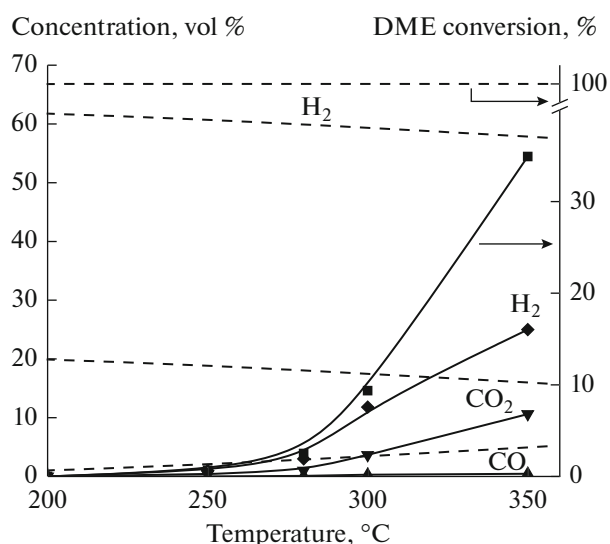


**Fig. 5.** Temperature dependencies of  $H_2$ ,  $CO_2$  and  $CO$  concentrations and DME conversion at DME SR on  $CuO-ZnO/\gamma-Al_2O_3$ . Experimental conditions: pressure 1 atm, GHSV  $10000\ h^{-1}$ , inlet mixture composition (vol %) DME :  $H_2O$  :  $N_2$  (20 : 60 : 20). Points stand for experiment, dotted lines stand for equilibrium values.

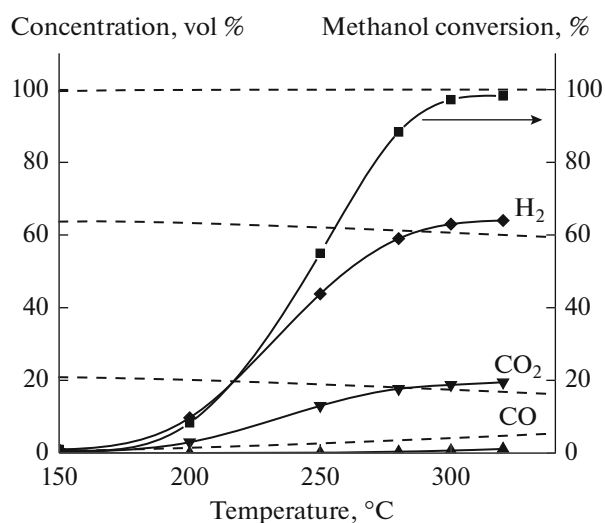


**Fig. 6.** Temperature dependencies of  $H_2$ ,  $CO_2$  and  $CO$  concentrations and methanol conversion at methanol SR on  $CuO-ZnO/\gamma-Al_2O_3$ . Experimental conditions: pressure 1 atm, GHSV  $10000\ h^{-1}$ , inlet mixture composition (vol %)  $CH_3OH$  :  $H_2O$  :  $N_2$  (40 : 40 : 20). Points stand for experiment, dotted lines stand for equilibrium values.

sions, and the outlet  $H_2$ ,  $CO_2$  and  $CO$  concentrations at DME and methanol SR on  $CuO-ZnO/\gamma-Al_2O_3$ . It is seen that the conversions and product concentrations increase with increasing temperatures in both reactions. In DME SR experiments (Fig. 5), the DME conversion and product concentrations considerably under-reach the equilibrium values in the temperature interval of 250–350°C. At higher temperatures, the catalyst shows unstable activity: the DME conversion and product concentrations fall with time. On the contrary, the catalyst performance in methanol SR (Fig. 6) was much better. As the temperature increased from 150 to 300°C, the methanol conversion attained the equilibrium value  $\sim 100\%$ . The  $H_2$  and  $CO_2$  concentrations slightly exceeded the equilibrium values, while the  $CO$  concentration ( $\leq 1$  vol %) remained below the equilibrium value. This tendency was observed in other works as well [10, 22], and is attributed most likely to the fact that  $H_2$  and  $CO_2$  are the primary products of reac-

tion (III), while  $CO$  is formed by reaction (V). Clearly, if reaction (V) does not reach equilibrium during the experiment, the  $H_2$  and  $CO_2$  concentration will exceed, while  $CO$  concentration remain below respective equilibrium values. Note that this tendency is similar to that observed in DMM SR.

The data obtained allow conclusion that  $CuO-ZnO/\gamma-Al_2O_3$  is an efficient catalyst for methanol SR to hydrogen-rich gas with low  $CO$  content. At 300°C, it provides  $\sim 100\%$  conversion of methanol with a hydrogen productivity of  $\sim 15\ L_{H_2}\ g_{cat}^{-1}\ h^{-1}$ , well competing the most active copper-based catalysts [12, 28, 29].

#### *Assessment of $CuO-ZnO/\gamma-Al_2O_3$ as a Catalyst for Multi-Fuel Processor*

The above data prove  $CuO-ZnO/\gamma-Al_2O_3$  to be an active and selective catalyst for DMM and methanol SR to hydrogen-rich gas. To estimate whether  $CuO-$

**Table 2.** Performance of  $CuO-ZnO/\gamma-Al_2O_3$  in methanol and DMM SR

Compound	Inlet mixture, vol %	$T, ^\circ C$	Concentration, vol %		$W_{H_2},$ $L_{H_2}\ g_{cat}^{-1}\ h^{-1},$
			$H_2$	$CO$	
$CH_3OH$	$CH_3OH : H_2O : N_2$ (40 : 40 : 20)	300	59.4	0.9	15
DMM	$DMM : H_2O : N_2$ (14 : 70 : 16)	280	60.5	0.9	16.5

Note: reaction conditions—pressure 1 atm, GHSV  $10000\ h^{-1}$ .

ZnO/ $\gamma$ -Al<sub>2</sub>O<sub>3</sub> is promising as a catalyst for multi-fuel processor (i.e., a unit capable to generate hydrogen-rich gas from various fuels under similar conditions using the same catalyst) applications, we compared its performance in DMM SR and methanol SR reactions. Table 2 presents the compared parameters: temperature ( $T$ ) at which  $\sim 100\%$  conversion of DMM and methanol was observed, the outlet H<sub>2</sub> and CO concentrations, hydrogen productivity ( $W_{H_2}$ ). It is seen that complete conversion of DMM and methanol was reached at 280 and 300°C, respectively, and the obtained gas contained almost the same amounts of hydrogen ( $\sim 60$  vol %) and CO ( $< 1$  vol %). The latter fact (low CO content) is especially attractive, because it means essential simplification of hydrogen-rich gas production scheme for PEM FC feeding. Indeed, the obtained mixture can be used for high-temperature PEM FC feeding without any special CO-cleanup procedures [1]. For low-temperature PEM FC feeding, CO removal to the level of  $< 10$  ppm is needed [2]. For this purpose, the processes of partial oxidation [30] or CO methanation [31, 32] are used; the step of WGS becomes unnecessary.

Hydrogen productivities of CuO–ZnO/ $\gamma$ -Al<sub>2</sub>O<sub>3</sub> in methanol and DMM SR are similar as well (15 and 16.5 L<sub>H<sub>2</sub></sub> g<sub>cat</sub><sup>-1</sup> h<sup>-1</sup>, respectively). That is, to provide operation of a 1 kW PEMFC-based power unit fuelled by DMM or methanol, ca. 50 g of the catalyst is needed.

Thus, the CuO–ZnO/ $\gamma$ -Al<sub>2</sub>O<sub>3</sub> bifunctional catalyst is quite efficient for DMM and methanol SR and shows high promises for using in a multi-fuel processor generating hydrogen-rich gas for PEM FC-based power units fueling.

## CONCLUSIONS

It is found that CuO–ZnO/ $\gamma$ -Al<sub>2</sub>O<sub>3</sub> is an active and selective catalyst for DMM and methanol SR producing hydrogen-rich gas with low CO content ( $< 1$  vol %). It provides complete conversion of methanol and DMM and hydrogen productivity of 15 and 16.5 L<sub>H<sub>2</sub></sub> g<sub>cat</sub><sup>-1</sup> h<sup>-1</sup>, respectively. The catalyst is promising for using in a multi-fuel processor generating hydrogen-rich from various fuels (methanol and DMM).

Physicochemical characterization and catalytic experiments proved the presence on the CuO–ZnO/ $\gamma$ -Al<sub>2</sub>O<sub>3</sub> surface of LAS typical for  $\gamma$ -Al<sub>2</sub>O<sub>3</sub> and 20–80 nm agglomerates comprised of copper and zinc oxide with atomic ratio Cu/Zn = 2. The former are responsible for DMM hydration to methanol and formaldehyde, the latter are responsible for methanol and formaldehyde SR to hydrogen-rich gas.

## ACKNOWLEDGMENTS

The authors are grateful to Dr. Zyuzin D.A. for assistance in a set of experiments. This work was conducted within the framework of budget project no. 0303-2016-0011 for Boreskov Institute of Catalysis.

## REFERENCES

1. Peighambardoust, S.J., Rowshanzamir, S., and Amjadi, M., *Int. J. Hydrogen Energy*, 2010, vol. 35, p. 9349.
2. Chandan, A., Hattenberger, M., El-kharouf, A., Du, S., Dhir, A., Self, V., Pollet, B.G., Ingram, A., and Bujalski, W., *J. Power Sources*, 2013, vol. 231, p. 264.
3. Mehta, V. and Cooper, J.S., *J. Power Sources*, 2003, vol. 114, p. 32.
4. O'Connell, M., Kolb, G., Schelhaas, K.-P., Wichert, M., Tiemann, D., Pennemann, H., and Zapf, R., *Chem. Eng. Res. Des.*, 2012, vol. 90, p. 11.
5. Idem, R. and Bakhshi, N.N., *Ind. Eng. Chem. Res.*, 1994, vol. 33, p. 2056.
6. Jones, S. and Hagelin-Weaver, H., *Appl. Catal., B*, 2009, vol. 90, p. 195.
7. Palo, D., Dagle, R., and Holladay, J., *Chem. Rev.*, 2007, vol. 107, p. 3992.
8. Yong, S., Ooi, C., Chai, S., and Wu, X., *Int. J. Hydrogen Energy*, 2013, vol. 38, p. 9541.
9. Li, D., Li, X., and Gong, J., *Chem. Rev.*, 2016, vol. 116, p. 11529.
10. Galvita, V., Semin, G., Belyaev, V., Yurieva, T., and Sobyenin, V., *Appl. Catal., A*, 2001, vol. 216, p. 85.
11. Vicente, J., Gayubo, A., Erena, J., Aguayo, A., Olazar, M., and Bilbao, J., *Appl. Catal., B*, 2013, vols. 130–131, p. 73.
12. Semelsberger, T., Ott, K., Borup, R., and Greene, H., *Appl. Catal., A*, 2006, vol. 309, p. 210.
13. Badmaev, S., Volkova, G., Belyaev, V., and Sobyenin, V., *React. Kinet. Catal. Lett.*, 2007, vol. 90, p. 205.
14. Volkova, G., Badmaev, S., Belyaev, V., Plyasova, L., Budneva, A., Paukshtis, E., Zaikovskiy, V., and Sobyenin, V., *Stud. Surf. Sci. Catal.*, 2007, vol. 167, p. 445.
15. Snytnikov, P., Badmaev, S., Volkova, G., Potemkin, D., Zyryanova, M., Belyaev, V., and Sobyenin, V., *Int. J. Hydrogen Energy*, 2012, vol. 37, p. 16388.
16. <http://huayan-formaldehyde.com/methylal.html>.
17. Zheng, Y., Tang, Q., Wang, T., and Wang, J., *Chem. Eng. Sci.*, 2015, vol. 134, p. 758.
18. Sun, Q., Auroux, A., and Shen, J., *J. Catal.*, 2006, vol. 244, p. 1.
19. Fu, Y. and Shen, J., *J. Catal.*, 2007, vol. 248, p. 101.
20. Shen, H., Fu, Y., Sun, Q., Zuo, S., Auroux, A., and Shen, J., *Catal. Commun.*, 2008, vol. 9, p. 801.
21. Badmaev, S.D., Pechenkin, A.A., Belyaev, V.D., Ven'yaminov, S.A., Snytnikov, P.V., Sobyenin, V.A., and Parmon, V.N., *Dokl. Phys. Chem.*, 2013, vol. 452, p. 251.

22. Pechenkin, A., Badmaev, S., Belyaev, V., and Sobyenin, V., *Appl. Catal., B*, 2015, vols. 166–167, p. 535.
23. Badmaev, S., Pechenkin, A., Belyaev, V., and Sobyenin, V., *Int. J. Hydrogen Energy*, 2015, vol. 40, p. 14052.
24. Paukshtis, E.A., *Infrakrasnaya spektroskopiya v geterogennom kislotno-osnovnom katalize* (Infrared Spectroscopy Applied to Heterogeneous Catalysis), Novosibirsk: Nauka, 1992.
25. Yahiro, H., Murawaki, K., Saiki, K., Yamamoto, T., and Yamaura, H., *Catal. Today*, 2007, vol. 126, p. 436.
26. Dow, W.-P., Wang, Y.-P., and Huang, T.-J., *J. Catal.*, 1996, vol. 160, p. 155.
27. Takezawa, N., *Catal. Today*, 1997, vol. 36, p. 45.
28. Oguchi, H., Nishiguchi, T., Matsumoto, T., Kanai, H., Utani, K., Matsumura, Y., and Imamura, S., *Appl. Catal., A*, 2005, vol. 281, p. 69.
29. Kühl, S., Friedrich, M., Armbrüster, M., and Behrens, M., *J. Mater. Chem.*, 2012, vol. 22, p. 9632.
30. Snytnikov, P.V., Potemkin, D.I., Rebrov, E.V., Sobyenin, V.A., Hessel, V., and Schouten, J.C., *Chem. Eng. J.*, 2010, vol. 160, p. 923.
31. Snytnikov, P.V., Zyryanova, M.M., and Sobyenin, V.A., *Top. Catal.*, 2016, vol. 59, p. 1394.
32. Konishcheva, M.V., Potemkin, D.I., Badmaev, S.D., Snytnikov, P.V., Paukshtis, E.A., Sobyenin, V.A., and Parmon, V.N., *Top. Catal.*, 2016, vol. 59, p. 1424.